

---

A Self-Powered Dual-Type Signal Vector Sensor for Smart Robotics and Automatic Vehicle

*Shaoxin Li, Zhihao Zhao, Di Liu, Jie An, Yikui Gao, Dr. Linglin Zhou, Yanhong Li, Shengnan Cui, Jie Wang\*, Zhong Lin Wang\**

S. Li, Dr. Z. Zhao, Dr. D Liu, J. An, Y. Gao, Dr. L. Zhou, Y. Li, S. Cui, Prof. J. Wang, Prof. Z. L. Wang

Beijing Institute of Nanoenergy and Nanosystems, Chinese Academy of Sciences, Beijing 100083, P. R. China

E-mail: wangjie@binn.cas.cn (J. Wang)

S. Li, Dr. Z. Zhao, Dr. D Liu, J. An, Dr. L. Zhou, S. Cui, Prof. J. Wang, Prof. Z. L. Wang

School of Nanoscience and Technology, University of Chinese Academy of Sciences, Beijing 100049, P. R. China

Prof. Z. L. Wang

School of Materials Science and Engineering, Georgia Institute of Technology, Atlanta, GA 30332, USA

This article has been accepted for publication and undergone full peer review but has not been through the copyediting, typesetting, pagination and proofreading process, which may lead to differences between this version and the [Version of Record](#). Please cite this article as [doi: 10.1002/adma.202110363](https://doi.org/10.1002/adma.202110363).

This article is protected by copyright. All rights reserved.

---

E-mail: zhong.wang@mse.gatech.edu (Z. L. Wang)

Keywords: self-powered vector sensor, real-time monitoring vector movement, triboelectric nanogenerator, automatic robotics, automatic vehicle.

---

**Abstract**

Automatic control system is the most efficient technology for reducing labor cost while improving work efficiency. Vector motion monitoring is indispensable for the normal operation of automatic control system. Here, we designed a self-powered dual-type signal triboelectric nanogenerator (DS-TENG) through integrating an alternative-current TENG and a direct-current TENG, which can monitor vector movement in real time based on pulse signal counts. As a result, the DS-TENG avoids the shortcoming of traditional self-powered sensors based on signal amplitude that is sensitive to the working environment, achieves a high sensing precision and maintains stability after reciprocating motion of 500,000 cycles. Moreover, it realizes effective movement direction recognition by self-powered switching of signal type in reverse movement. This dual-type signal TENG exhibits high precision and automatic direction recognition in vector motion monitor and trajectory tracker, paving the way for the application of self-powered TENG sensor in automatic control system in the future.

---

## 1. Introduction

As the automatic control system develop rapidly, the conventional working mode is being subverted. It contributes to the development of automatic factories, driverless cars, and self-service technologies and so on for replacing human beings to complete dangerous and tedious work, while maintaining high standardization and precision.<sup>[1]</sup> In order to ensure the normal operation or supervise equipment failure of automatic control system, vector sensors are essential in the automated process to obtain vector motion parameters (movement direction, displacement, angle, velocity, acceleration and so on).<sup>[2]</sup> Currently, some commercialized vector sensors have been proposed based on Hall effect, piezoelectric effect and photoelectric effect.<sup>[3]</sup> However, the dependence on external power limits their application in distributed arrays of sensors. Besides, the coaxial photoelectric transmitter, optical grating, and receiver of traditional grating angular sensor will inevitably increase its thickness and weight. Two synchronous photoelectric detectors are required to achieve direction recognition based on phase difference principle, otherwise the crosstalk between of them will cause the wrong direction feedback. Considering the above constrains, it is highly desirable to develop a self-powered, lightweight vector motion monitoring system.

In recent years, various kinds of self-powered vector sensors based on triboelectric nanogenerator (TENG) have been proposed, because its alternating current (AC) signal amplitudes are sensitive to the changes in external movement state (*e.g.*, distance, acceleration, velocity).<sup>[4]</sup> However, the AC signal amplitude is also extremely susceptible to the unstable environment (*e.g.*, temperature, humidity), resulting in the degradation of its precision.<sup>[5]</sup> Meanwhile, the principle of direction recognition of traditional self-powered sensors in vector motion monitoring, namely phase difference principle, is similar to that of grating angular sensor. It also requires complex multi-electrode structure and multichannel signal transmission, which may cause crosstalk between different channels.

---

In this work, we integrated a DC-TENG and an AC-TENG to design a dual-type signal triboelectric nanogenerator (DS-TENG) sensor based on triboelectrification, electrostatic induction, and electrostatic breakdown. Our sensor realizes pulse-signal counting and the fast switching of two-type pulse signal in reverse movement, which further improves the stability of precision and simplifies the process of motion direction recognition. Additionally, a linear sensor (DSL-TENG) with precision of 500  $\mu\text{m}$  and angular sensor (DSA-TENG) with precision of  $2^\circ$  are implemented, enabling vector linear and rotate motion monitoring, as well as their theoretical minimum resolution can reach 6.79  $\mu\text{m}$  and  $0.12^\circ$ , respectively. After comprehensive optimization with the help of micromachining process and stronger electronegativity material, the precision of DS-TENG can be further improved in future. Meanwhile, the precision of DS-TENG sensor is not sensitive to the variation of temperature and humidity, and maintains stable after reciprocating motion of 500, 000 cycles. Apart from generating AC signal in one motion direction, DS-TENG sensor also generates direct current (DC) signal in another motion direction. Benefiting from the rapid switching of two-type signal in reverse movement, DS-TENG sensor makes the judgement process of motion direction more precise and faster. With the advantages of self-powered, high precision and simple motion directional recognition technologies, DS-TENG sensor realizes the real-time trajectory tracking of robot body movement and driving direction monitoring of vehicle, showing great application prospects in the field of smart robot and automatic vehicle.

## **2. Results and Discussion**

### **2.1 The Structure and Mechanism of Dual-Type Signal Vector Sensor**

Automatic control system is helpful for people to withdrew from some complex, repetition and tedious working environment, which can reduce the labor supervision cost and

---

improve work efficiency. For example, the automated vehicle can alleviate traffic congestion and make the driver enjoy journey, which is essential to maintain good traffic order and reduce the incidence of traffic accidents (**Figure 1a**).<sup>[6]</sup> However, continuous real-time monitoring of angle and direction of steering wheel in automatic vehicle is still a huge challenge.<sup>[7]</sup> Here, we designed a self-powered dual-type pulse signal angular sensor, which can convert motion variables into electrical signal directly, and switch two types of electrical signal (AC or DC) in different motion directions (Figure 1b). Unlike traditional complex grating sensor needing external energy supply, stable light source and multi-detector design (Figure 1c), our self-powered sensor has different types of pulse signal in reverse movement, making the vector motion monitoring more effective and accurate (Figure 1d). In addition, the DS-TENG sensor has advantages of lower weight and thinner thickness compared with traditional photoelectric angular sensor (Figure S1, Supplementary Information). This further suggests that the miniaturized and lightweight DS-TENG sensor is more suitable for applications in space with limited volume and weight.

The detailed principle of DS-TENG is shown in Figure 1e, where the generation of DC signal in one rotate angle ( $\theta$ ) can be divided into four stages (take clockwise as example first).  
Triboelectrification stage (Figure 1e(i)): when fluorinated ethylene propylene (FEP) as friction layer (FL) contacts with copper foil as friction electrode (FE), opposite and equal charges are distributed on their surfaces because of the contact triboelectrification effect.<sup>[8]</sup>  
Air breakdown stage (Figure 1e(ii)): once the negative charged FL slips out of the boundary of FE, a strong electrostatic field will be established in the tiny gap ( $\sim 30 \mu\text{m}$ ) between FL and charge collecting electrode (CCE), causing air breakdown based on Paschen's law, which is proved by COMSOL simulation (Figure S2, Supplementary Information). With the help of breakdown channel, electron always transfers from CCE to FE through external circuit, thus generating DC signal.<sup>[9]</sup>  
DC blocking stage (Figure 1e(iii)): when FL slides completely over

---

FE, the strong electrostatic field in the gap disappears, namely the breakdown channel is cut off. Re-triboelectrification stage (Figure 1e(iv)): most negative charges on the surface of FL have been released during the discharge process of air breakdown. Thus, when FL continuously rotates clockwise and contacts with FE, triboelectrification will happen again and the next motion cycle will generate a new periodic pulse signal. Therefore, the number of DC pulses corresponds to rotation angle of the DS-TENG sensor.

While during the countermotion (counterclockwise rotate) process, DS-TENG produces AC signal due to the effects of triboelectrification and electrostatic induction. The detailed mechanism is also divided into four parts, the first stage is triboelectrification stage (Figure 1f(i)), which is same as Figure 1d(i); Potential non-conservation stage (Figure 1f(ii)): the contact area between of FE and FL decreases as the FL gradually slipping out of FE, and the electron transfers from CCE to FE to balance the potential difference between them. To avoid excess charges on the surface of FL forming breakdown channel in that tiny gap, a DC filtering electrode (DCFE) is grounded to decrease the electrostatic field strength between FL and CCE, thus reducing the interference for next stage. The comparison results between the DSA-TENG with and without DCFE indicates AC is generated in DSA-TENG with DCFE, while the other signal is disorganized with many breakdown signals (Figure S3, Supplementary Information). Potential maximization stage (Figure 1f(iii)): the relative contact area between FE and FL reaches the minimum, and their potential difference reaches the maximum, the corresponding COMSOL simulation result is shown in Figure S4, Supplementary Information. Potential reverse non-conservation stage (Figure 1f(iv)): the contact area between FE and FL increases as the FL gradually slides, and the electron transfers from FE to CCE to balance the potential difference between them.<sup>[10]</sup>

As mentioned above, taking advantage of structural design, DS-TENG sensor generates AC or DC pulse signal in reverse movement without external energy supply. Moreover,

---

pulse-signal counting method, here the number of AC or DC pulse counts corresponds to the rotation angle, for self-powered system can effectively improve the sensing accuracy of the sensor.<sup>[11]</sup>

## 2.2 Structural Optimization of DS-TENG Sensor in Linear Motion

The structure of DS-TENG suitable for linear motion monitoring (DSL-TENG) is shown in **Figure 2a**. When DSL-TENG moving to the left (the FE is in front of CCE is behind), the triboelectrification effect occurs firstly, and then the air breakdown happens, resulting in a DC sensing signal. While in the movement to the right (the CCE is in front of FE), it forms AC signals without DCFE based on triboelectrification and electrostatic induction. To generate count pulse sensing signal, periodic grading structure has been etched on the surface of FEP by laser cutting machine. The minimum scale grid period of FEP is 500  $\mu\text{m}$ , indicating that each pulse signal represents a motion displacement of 500  $\mu\text{m}$  (other sensing precisions of 1 mm and 2 mm are shown in Figure S5, S6, Supplementary Information, and the demonstration of real-time monitoring in vector motion is shown in Movie S1, Supplementary Information. The original current signal of DSL-TENG sensor is shown in Figure 2b, where 10 DC pulse peaks appear when the slider moves 5 mm to the left, and 10 AC pulse peaks appear when it moves to the right to the initial position. In this process, the corresponding DC voltage and AC voltage of DSL-TENG sensor are shown in Figure 2c and 2d, respectively. The DC voltage occurs when CCE slides over the negatively charged FEP (air breakdown area), and disappears in the etched FEP (blank area). When DSL-TENG moves to right, the AC voltage, whose period is corresponded to the period of grid, is originated from the change of relative friction area. Similarly, the corresponding charge signal in that process is shown in Figure S7, Supplementary Information. It can be seen from Figure 2e that the denser grid period structure, the higher displacement precision of DSL-TENG sensor. Additionally, Figure S8, Supplementary Information shows the precision

of DSL-TENG sensor is not affected by the asymmetry of etched area and unetched regions within the same grid period, which is further verified the precision of DSL-TENG sensor only depends on the grid period rather than unetched region, although the area of unetched region will affect the peak value of current signal. Here, we chose the carving power of 2.3 Watt to fabricate groove grids of 500  $\mu\text{m}$  on the surface of FEP (Figure S9, Supplementary Information). According to the following equation,<sup>[12]</sup> the theoretical displacement precision can reach to 1.68  $\mu\text{m}$  (DC signal) and 6.79  $\mu\text{m}$  (AC signal), respectively (Figure S10, Note S1, Supplementary Information).

$$S = \frac{\Delta S}{\Delta I / I_{Noise}^{RMS}} \quad (1)$$

where  $S$  is the theoretical minimum resolvable displacement,  $\Delta S$  is the practical minimum resolvable displacement in this work,  $\Delta I$  is the current variance corresponding to  $\Delta S$ , and the  $I_{Noise}^{RMS}$  is the Root Mean Square (RMS) of the noise signal. It can be seen that reducing  $\Delta S$  and increasing  $\Delta I$  both are helpful to improve the precision of sensor. Taking advantage of the micromachining technology, the device with fine and appropriate surface structure can be produced to reduce  $\Delta S$  (Figure S11, Supplementary Information). Meanwhile, friction materials with more electronegativity and better mechanical performance can increase  $\Delta I$  (Note S2, Supplementary Information).<sup>[13]</sup>

Under different precisions of DSL-TENG, Figure 2f and 2g indicate that the experimental data of position and velocity are in line with their theoretical data. In addition, under different velocities, the calculated position and velocity from original current data in the Figure 2h are also accorded with the corresponding pre-set values (Figure 2i and 2j). This verified that the precision of 500  $\mu\text{m}$  can be maintained at different motion velocities. From Figure S12, Supplementary Information, we can see the reliability of DSL-TENG with high precision (500  $\mu\text{m}$ ) in long-distance or short-distance monitoring. Moreover, it can be seen

---

from Supplementary Figure 13 that the precision of DSL-TENG sensor keeps stable after reciprocating motion of 500,000 cycles (detailed description in Note S3, Supplementary Information). Apart from self-powered monitoring of displacement and velocity, DSL-TENG sensor can effectively and accurately judge the movement direction of an object via the fast switching of different type signals, thus obtaining its motion trajectory, as shown in Movie S2, Supplementary Information. From the signal of Figure S14 and Note S4, Supplementary Information, it can be inferred that the DSL-TENG slider moves 10 mm to the right from the starting position (corresponding to 5 AC pulses), then moving 30 mm to the left (corresponding to 15 DC pulses), next moving 30 mm to the right (corresponding to 15 AC pulses). Finally, the final position is 10 mm to the right of the starting position. This inferred trajectory is completely consistent with the pre-set motion process, proving the reliability of DSL-TENG in the real-time monitoring of trajectory.

### 2.3 Output Performance of DS-TENG in Angular Sensor

To expand the application scenarios of TENG sensor in automatic control system, we fabricated a self-powered DS-TENG as an angular sensor (DSA-TENG), whose structural design is shown in **Figure 3a**. The original current signal of DSA-TENG sensor during rotation reciprocating motion of  $50^\circ$  is shown in Figure 3b, where each pulse peak represents  $10^\circ$ , the DC signal represents clockwise rotation, and the AC signal represents counterclockwise rotation. Since the angular position and angular velocity calculated from Figure 3b match the pre-set values (Figure 3c and 3d), the DSA-TENG sensor is reliable to monitor rotational motion. It is worth noting that an interspace is designed on rotator to add a DCFE, so that preventing air breakdown in counterclockwise rotation. The influence of interspace angle on the performance of DSA-TENG is shown in Figure S15, Supplementary Information, where the output of sensing signals increases initially and decreases afterward as

the angle of interspace increases. Considering the flexibility of FEP film and the electric field between CCE and DCFE, we chose the interspace of  $45^\circ$  to design DSA-TENG. The output performance of DSA-TENG sensor can be enhanced by increasing the number of CCE (Figure S16, Supplementary Information). Additionally, we also improve the precision of DSA-TENG sensor to  $5^\circ$  and even  $2^\circ$  through subdividing the grid period of FEP on the circular outer ring. Detailed sensing performances of DSA-TENG with the precision of  $5^\circ$  and  $2^\circ$  at different angular velocities are shown in Figure S17, S18, Supplementary Information. The calculated position and angular velocity of DSA-TENG sensor with different precisions in Figure 3e show good relationship with the pre-set values (Figure 3f and 3g). In theory, according to equation (1), the angle precision of DSA-TENG sensor can reach to  $0.024^\circ$  (DC signal) and  $0.12^\circ$  (AC signal). Its noise current signal and detailed calculation process are shown in Figure S19, Note S1, Supplementary Information, respectively. As shown in Figure 3h and 3j, at the same rotation velocity of  $144^\circ \text{ s}^{-1}$ , the amplitude of signal changes with the increase of temperature and humidity. However, the calculated rotation velocity is matched with the pre-set one, which further verifies that the precision of DSA-TENG sensor based on pulse signal counts is not affected by the changes in working environment (Figure 3i and Figure 3k). Furthermore, the comparison of sensing performance of our sensor and recently vector sensor based on triboelectrification is shown in Table S1, Supplementary Information.

## 2.4 Application of DSA-TENG Sensor in Smart Robotics

The working diagram of DSA-TENG sensor applied in real-time monitoring of the joint motion of mechanical arm is presented in **Figure 4a**. The motion of mechanical joint makes DSA-TENG sensor generate corresponding electrical signals. According to the characteristic of output signal, *e.g.*, signal type, pulse counts and pulse width, we can obtain the rotation

---

direction, angle, and velocity. Figure 4b(i) shows the photo of DSA-TENG sensor combined with mechanical arm. Figure 4b(ii) is the disassembly diagram of the arm protector, and the detailed enlarged photos of DSA-TENG sensor are shown in Figure 4b(iii) and 4b(iv). In Figure 4c, the DC signal represents clockwise rotation, while the AC signal represents counterclockwise rotation. Through analyzing the pulse counts and pulse width, the motion trajectory of elbow can be monitored in real-time (the detailed dynamic movie is shown in Movie S3, Supplementary Information). In the initial posture, the angle between the upper and lower arm is  $175^\circ$ . When the elbow gradually bends to an angle of  $135^\circ$  between the two arms, the electrical signal with 8 DC pulse peaks is generated, corresponding to  $40^\circ$  of arm bending (Figure 4c(i)). The next 6 DC pulse peaks indicate that the elbow continues to bend  $30^\circ$ . Accumulating the rotation angle of previous stage, the arm is bend  $70^\circ$  relative to the initial stage (Figure 4c(ii)), so the angle between two arms is  $105^\circ$ . Then, the arm gradually straightens to an angle of  $135^\circ$ , and the 6 AC pulse peaks correspond to a counterclockwise rotation angle of  $30^\circ$  (Figure 4c(iii)). In the end, the elbow bends  $30^\circ$  relative to last stage, so 6 AC pulse peaks have been detected (Figure 4c(iv)). Through analyzing the characteristics of electrical signal from DSA-TENG, it not only can detect the motion state of measured object, but also monitor the continuous trajectory of arm. This self-powered sensing and self-diagnostic function of DSA-TENG sensor is conducive to the real-time movement monitoring and motor trajectory tracking of smart robotics. Beyond that, it also might be applied in the field of human medical rehabilitation through regular monitoring of joint movement.

## 2.5 Application of DSA-TENG Sensor in Automatic Vehicle

The traffic congestion and driving fatigue of drivers can be greatly alleviated by the automatic vehicle technology.<sup>[14]</sup> To guarantee driving safety, angular sensor plays an

---

important role in automatic vehicle through real-time monitoring and feedback of the vehicle information. Here, we integrated the DSA-TENG sensor into the automatic control system of car steering wheel to monitor its rotation angle and direction (**Figure 5a**). It can be seen from Figure 5b that software interface controls the steering wheel and receives the sensing signal. The working process of DSA-TENG is shown in Figure 5c. The steering wheel moves according to the command preset by the computer, while computer receives the sensing signal from DSA-TENG fixed on the steering wheel. Through data acquisition card (DAC), physical quantity of motion, *e.g.*, rotation direction, angle, and angular velocity, can be obtained based on the type, pulse counts, and pulse width of the sensing signal.

Figure 5d and 5e are the comparison of actual automatic driving rotation motion and sensing signal from DSA-TENG sensor, respectively. The initial state of the wheel faces the front of the car. DC signal is generated when wheels turn to the left (clockwise rotation, blue-line flow in Figure 5d and blue area in Figure 5e), while the AC signal is produced when turning to the right (counterclockwise rotation, red-line flow in Figure 5d and red area in Figure 5e). Every electrical signal corresponds to a certain motion process. Thus, we can trace the movement of steering wheel, and the detailed dynamic demonstration process is shown in Movie S4, Supplementary Information. In summary, an automatic direction sensing system based on DSA-TENG can be divided into automatic driving program and information feedback (Figure 5f). The automatic driving program pre-inputs certain algorithms or codes to control the direction of the car's movement, and the feedback is obtained by computer analysis of the sensing signal from DSA-TENG. Thus, the DSA-TENG sensor achieves the real-time monitoring and information feedback of steering wheel. This can be further applied to automatic vehicle systems to track vehicle trajectory in real time to ensure driving safety.

### 3. Conclusion

---

We proposed a self-powered and stable triboelectric nanogenerator vector sensor for monitoring linear or rotational motion in automatic control system. Based on the sensing principle of pulse signal counts, the decrease of precision caused by non-linear amplitude under changed environment has been solved. Besides, the precision of DS-TENG still keeps stable after 500, 000 reciprocating cycles. Thanks to the unique structural, DS-TENG can generate different signal types (AC or DC) in reverse movement. As demonstrated, DS-TENG can be applied in automatic control system for real-time monitoring of linear or rotational vector motion. According to the characteristics of signal type, pulses counts, pulses width, we can obtain movement parameters, *e.g.*, the move direction, displacement, angle, velocity, and angular velocity. We also preliminarily achieved the real-time monitoring and motion trajectory tracking of mechanical arm and steering wheel movements of automatic vehicle by DSA-TENG sensor. In future work, the precision of DS-TENG sensor can be further improved by micromachining technology and better triboelectrification material. This work not only significantly improves the precision stability of self-powered sensors and proposes a new method of movement direction recognition through unique structural design, but also demonstrates the application potential of TENG sensor in smart robotics and automatic vehicle technology.

## 4. Methods

### 4.1 Fabrication of the DSL-TENG

The DSL-TENG sensor is consist of slider and grid rail. The fabrication of slider: (1) Choose an acrylic with thickness of 5 mm as the substrate material, and the size of acrylic (20 mm × 20 mm) is cut by a laser cutter (PLS6.75 Universal Laser System); (2) Attach the same size (20 mm × 20 mm) of copper foil (thickness 30 μm) to substrate, and this copper foil is called

---

friction electrode; (3) Attach a 20 mm × 5 mm of copper foil (thickness 30 μm) to the side of substrate as the charge collecting electrode. The fabrication of grid rail: (1) Fix the same size FEP film with high temperature resistance (thickness: 150 μm) on the acrylic substrate (size: 100 mm × 30 mm); (2) Carve the periodical grid structure (grid period: 0.5 mm, 1 mm, 2 mm) on the surface of FEP through laser cutter. Here, we choose the carving power of 2.3 Watt to fabricate groove grids on the surface of FEP.

#### 4.2 Fabrication of the DSA-TENG

The DSA-TENG is consist of rotor and stator. The fabrication of rotor: (1) Fix the same size FEP film (thickness:150 μm) on the acrylic circular substrate (diameter: 30 mm or 50 mm). A thin layer of foam (thickness: ~0.5 mm) can be added between the acrylic and FEP film to improve contact efficiency of friction electrode and FEP film. (2) Carve the periodical grid structure (grid period: 2°, 5°, 10°) on the surface of FEP through laser cutter (carving power: ~2.3 W). The fabrication of stator: (1) Cut a fan-shaped interspace of 45° in the circular substrate; (2) Put a copper foil (thickness: 30 μm) on the base plane of the substrate as friction electrode. For reducing the manual preparation, the step (1) and (2) can be combined by the mature printed circuit board (PCB) technology. (3) Attach the same size copper foil on the two side of fan-shaped hole, and ground one of them as DC filtering electrode, the other as charge collecting electrode.

#### 4.3 Experimental Setup for Linear and Rotator Parameter Control and Electrical Measurement.

---

The linear motion procession: fix the grid rail on a fixed lifting platform, and the slider fixed on the linear motor (LinMot BF01-37) to moves in a linear motion. The motion parameter is controlled by computer. The rotation process: fix the rotor on the shaft of stepping electric rotating machine (MODEL 86HSE8.5N-B32), and the stator on a fixed lifting platform. The rotate motion parameter is controlled by stepper motor controller. A programmable electrometer (Keithley Instruments model 6514) is adopted to measure the current, voltage and charge signal of DS-TENG.

### **Supporting Information**

Supporting Information is available from the Wiley Online Library or from the author.

### **Acknowledgements**

S. L., Z. Z. and D. L. contributed equally to this work. Research was supported by the National Key R & D Project from Minister of Science and Technology (2021YFA1201602), National Natural Science Foundation of China (Grant no. 61774016, 22109013), Fundamental Research Funds for the Central Universities (E1E46802) and China Postdoctoral Science Foundation (2021M703172).

### **Conflict of Interest**

All authors have no declare financial/commercial conflicts of interest.

---

**References**

- [1] a) O. Kaynak, H. Luo and S. Yin, *IEEE Trans. Syst. Man Cybern. Syst.* **2020**, *50*, 3330; b) I. Santana, M. Ferre, E. Izaguirre, R. Aracil, L. Hernandez, *IEEE Trans. Ind. Inform.* **2013**, *9*, 547.
- [2] a) Q Jing, Y Xie, G Zhu, R. P. S Han, Z L Wang, *Nat. Commun.*, **2015**, *6*, 1; b) C. Becker, D. Karnaushenko, T. Kang, D. D Karnaushenko, M. Faghih, A. Mirhajivarzaneh, O. G Schmidt, *Sci. Adv.* **2019**, *5*, eaay7459; c) X. Yin, D. Liu, L. Zhou, X. Li, G. Xu, L. Liu, S. Li, C. Zhang, J. Wang, Z. L. Wang, *Adv. Funct. Mater.* **2020**, *30*, 2002547.
- [3] a) Y. H. Jung, S. K. Hong, H. S. Wang, J. H. Han, T. X. Pham, H. Park, J. Kim, S. Kang, C. D Yoo, K. J. Lee, *Adv. Mater.* **2020**, *32*, e1904020; b) G. S. Kulkarni, W. Zang, Z. Zhong, *Acc. Chem. Res.* **2020**, *15*, 917-925; c) J. Yun, N. Jayababu, D. Kim, *Nano Energy* **2020**, *78*, 105325.
- [4] a) H. Ouyang, Z. Li, M. Gu, Y. Hu, L. Xu, D. Jiang, S. Cheng, Y. Zou, Y. Deng, B. Shi, W. Hua, Y. Fan, Z. Li, Z. L. Wang, *Adv. Mater.* **2021**, *33*, 2102302; b) H. Guo, X. Pu, J. Chen, Y. Meng, M.-H. Yeh, G. Liu, Q. Tang, B. Chen, Di Liu, Song Qi, C. Wu, C. Hu, J. Wang, Z. L. Wang, *Sci. Robot.* **2018**, *3*, eaat2516; c) Y. Wu, Y. Li, Y. Zou, W. Rao, Y. Gai, J. Xue, L. Wu, X. Qu, Y. Liu, G. Xu, L. Xu, Z. Liu, Z. Li, *Nano Energy*, **2022**, *92*, 106715; d) X. Qu, X. Ma, B. Shi, H. Li, L. Zheng, C. Wang, Z. Liu, Y. Fan, X. Chen, Z. Li, Z. L. Wang, *Adv. Funct. Mater.*, **2021**, *31*, 2006612; e) J. An, Z. Wang, T. Jiang, P. Chen, X. Liang, J. Shao, J. Nie, M. Xu, Z. L. Wang, *Mater. Today*, **2020**, *41*, 10. f) J. An, P. Chen, Z. Wang, A. Berbille, H. Pang, Y. Jiang, T. Jiang, Z. L. Wang, *Adv. Mater.* **2021**, *33*, 2101891.
- [5] S. Lin, L. Xu, C. Xu, X. Chen, A. C. Wang, B. Zhang, P. Lin, Y. Yang, H. Zhao, Z. L. Wang, *Adv. Mater.* **2019**, *31*, 1808197.

- 
- [6] a) D. Maurya, S. Khaleghian, R. Sriramdas, P. Kumar, R. A. Kishore, M. G. Kang, V. Kumar, H. -C. Song, S. -Yi Lee, Y. Yan, J. -M. Park, S. Taheri, S. Priya, *Nat. Commun.* **2020**, *11*, 5392; b) H. Askari, A. Khajepour, M. B. Khamesee, Z. L. Wang, *Nano Energy* **2019**, *66*, 104103; c) H. Askari, E. Hashemi, A. Khajepour, M.B. Khamesee, Z. L. Wang, *Nano Energy* **2018**, *53*, 1003.
- [7] M. Pan, C. Yuan, X. Liang, J. Zou, Y. Zhang, C. Bowen, *iScience* **2020**, *23*, 101682.
- [8] a) C. Xu, Y. Zi, A. C. Wang, H. Zou, Y. Dai, X. He, P. Wang, Y. -C. Wang, P. Feng, D. Li, and Z. L. Wang, *Adv. Mater.* **2018**, *30*, e1706790; b) L. Zhou, D. Liu, J. Wang, Z. L. Wang, *Friction* **2020**, *8*, 481; c) S. Lin, L. Xu, L. Zhu, X. Chen, Z. L. Wang, *Adv. Mater.* **2019**, *31*, 1901418.
- [9] a) S. Xu, H. Guo, S. L. Zhang, L. Jin, W. Ding, X. Wang, Z. L. Wang, *Appl. Phys. Lett.* **2020**, *116*, 263901; b) D Liu, X. Yin, H. Guo, L. Zhou, X. Li, C. Zhang, J. Wang, Z. L. Wang, *Sci. Adv.* **2019**, *5*, eaav6437; c) Y. Gao, D. Liu, L. Zhou, S. Li, Z. Zhao, X. Yin, S. Chen, Z. L. Wang, J. Wang, *Nano Energy* **2019**, *85*, 106014; d) J. Luo, L. Xu, W. Tang, T. Jiang, F. R. Fan, Y. Pang, L. Chen, Y. Zhang, Z. L. Wang, *Adv. Energy Mater.* **2018**, *8*, 1800889.
- [10] a) Y. Yang, Y. S. Zhou, H. Zhang, Y. Liu, S. Lee, Z. L. Wang, *Adv. Mater.* **2013**, *25*, 6594; b) Y. Yang, H. Zhang, J. Chen, Q. Jing, Y. S. Zhou, X. Wen, Z. L. Wang, *ACS nano* **2013**, *7*, 7342.
- [11] a) M. Xu, Y. -C. Wang, S. L. Zhang, W. Ding, J. Cheng, X. He, P. Zhang, Z. Wang, X. Pan, Z. L. Wang, *Extreme Mech. Lett.* **2017**, *15*, 122; b) H. Lin, Y. Liu, S. Chen, Q. Xu, S. Wang, T. Hu, P. Pan, Y. Wang, Y. Zhang, N. Li, Y. Li, Y. Ma, Y. Xie, L. Wang, *Nano Energy* **2019**, *65*, 103944; c) Q. Xu, Y. Fang, Q. Jing, N. Hua, K. Lin, Y. Pan, L. Xu, H.

- 
- Gao, M. Yuan, L. Chu, Y. Ma, Y. Xie, J. Chen, L. Wang, *Biosens. Bioelectron.* **2021**, *187*, 113329.
- [12] Z. Wang, J. An, J. Nie, J. Luo, J. Shao, T. Jiang, B. Chen, W. Tang, Z. L. Wang, *Adv. Mater.* **2020**, *32*, 2001466.
- [13] a) Z. Zhao, L. Zhou, S. Li, D. Liu, Y. Li, Y. Gao, Y. Liu, Y. Dai, J. Wang, Z. L. Wang, *Nat. Commun.* **2021**, *12*, 4686; b) L. Zhou, D. Liu, Z. Zhao, S. Li, Y. Liu, L. Liu, Y. Gao, Z. L. Wang, J. Wang, *Adv. Energy Mater.* **2020**, *10*, 2002920; c) C. Chen, Z. Wen, J. Shi, X. Jian, P. Li, J. T W Yeow, X. Sun, *Nat. Commun.* **2020**, *11*, 4143; d) L. Zhou, D. Liu, S. Li, Z. Zhao, C. Zhang, X. Yin, L. Liu, S. Cui, Z. L. Wang, J. Wang, *Adv. Energy Mater.* **2020**, *10*, 2000965; e) Z. Zhao, Y. Dai, D. Liu, L. Zhou, S. Li, Z. L. Wang, J. Wang, *Nat. Commun.* **2020**, *11*, 6186; f) L. Zhou, Y. Gao, D. Liu, L. Liu, Z. Zhao, S. Li, W. Yuan, S. Cui, Z. L. Wang, J. Wang, *Adv. Energy Mater.* **2021**, 2101958.
- [14] a) A. X. Lobo, *Transport Reviews* **2010**, *30*, 701; b) M. Fogue, P. Garrido, F. Martinez, J. -C. Cano, C. Calafate, P. Manzoni, *IEEE Veh. Technol. Mag.* **2012**, *7*, 90.

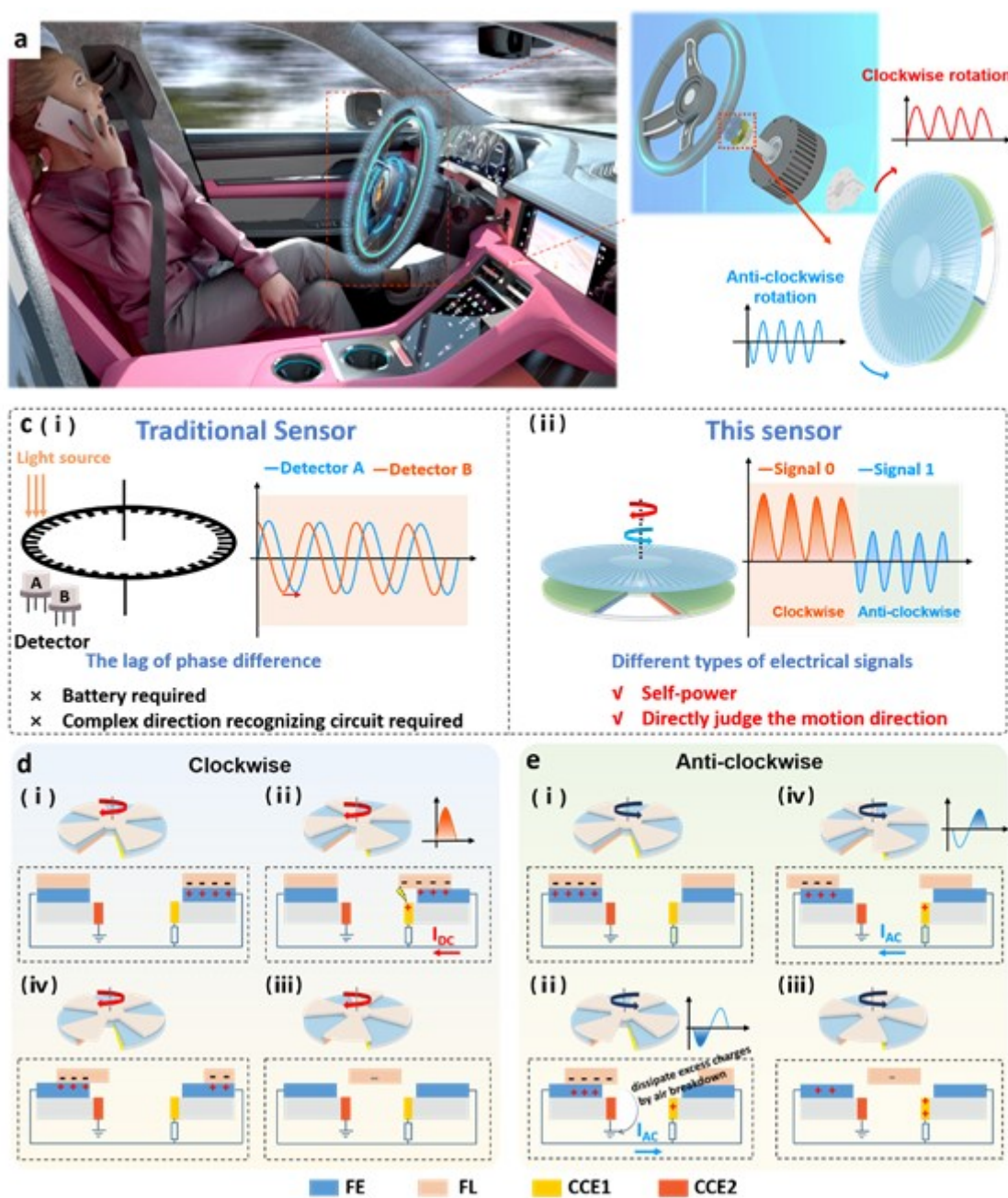


**Figure 1.** The structure and mechanism of dual-type signal TENG (DS-TENG). a) The concept application of DS-TENG. b) The magnified image of the selected area in diagram (a) to exhibit the installation position of DS-TENG, and further zoom in the detail structure of DS-TENG. c) The characteristics of traditional sensor in rotation motion monitoring. d) The

---

advantages of our sensor in rotation motion monitoring. e) The working mechanism of direct current (DC) signal generated by DS-TENG in one rotate angle  $\theta$  (take the clockwise rotation for example). f) The working mechanism of alternating current (AC) signal generated by DS-TENG in the counterclockwise rotation.

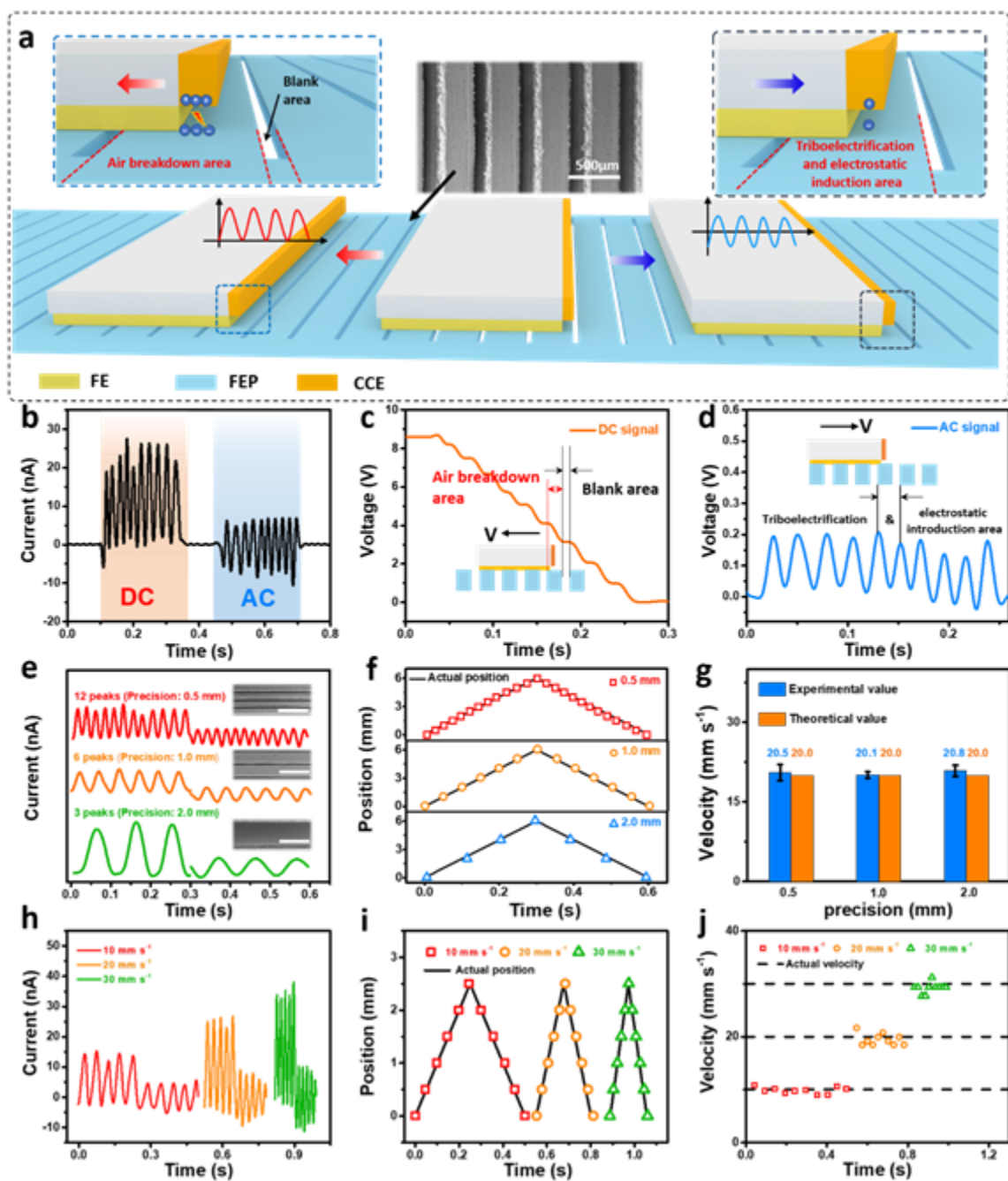


**Figure 2.** The structural optimization and characterizations of dual-type signal TENG in linear motion (DSL-TENG sensor). a) The structure and working mechanism of DSL-TENG sensor. Scale bar, 500  $\mu\text{m}$ . b) The original current signal of DSL-TENG sensor with precision

---

of 500  $\mu\text{m}$ , motion distance of 5 mm and velocity of 20 mm s<sup>-1</sup> in reverse movements. c) The DC voltage signal and d) AC voltage signal of DSL-TENG sensor at the same situation of diagram b in reverse movements respectively. e) The current signal generated by DSL-TENG sensor with different precisions (0.5 mm, 1 mm, 2 mm) but same displacement and velocity (6 mm and 20 mm s<sup>-1</sup>). Scale bar, 2 mm. f) Calculated positions and g) velocities from the experimental data in diagram (e), and their comparisons with the pre-set value. h) Current signal generated at the DSL-TENG sensor with 0.5 mm precision at various velocities but same displacement (2.5 mm). i) Calculated positions and j) velocities from the experimental data in the diagram (h), and their comparisons with the pre-set value.

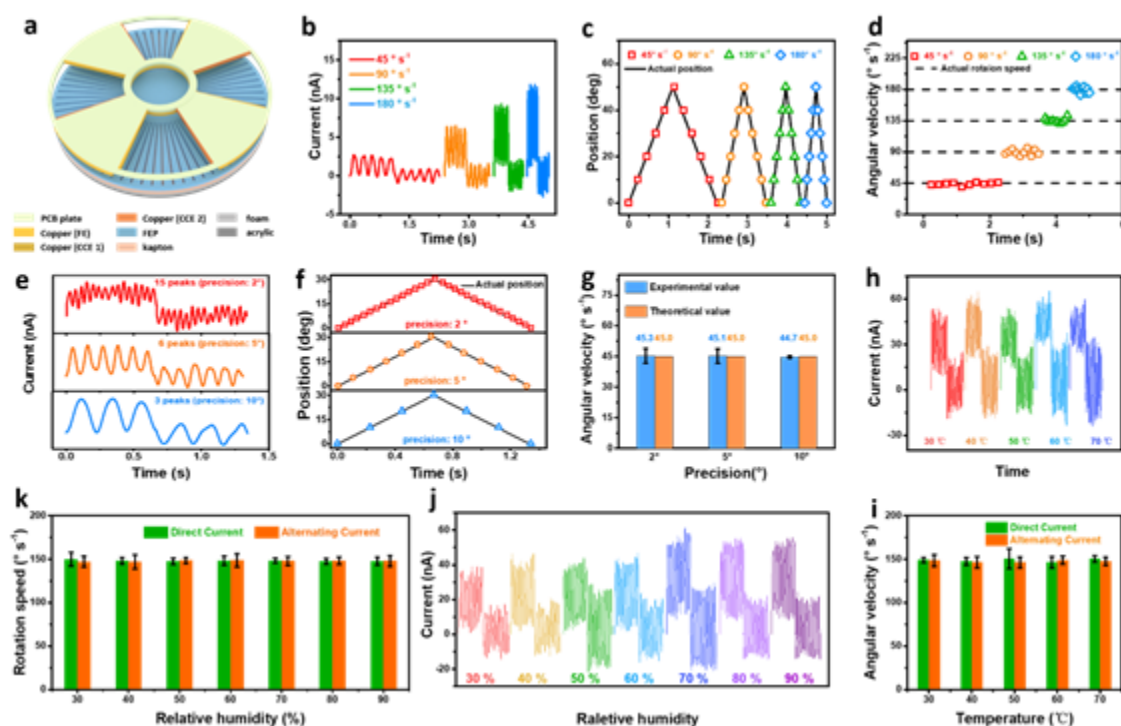


**Figure 3.** The output performance of dual signal angular sensor (DSA-TENG sensor). a) The structure representation of DSA-TENG sensor. b) The current signal of DSA-TENG sensor at precision of 10°, rotation angle of 50° with various angular velocities in reverse rotational movement. c), d) Calculated positions and angular velocity from the experimental data in the diagram (b), and their comparisons with the pre-set value. e) The current signal of DSA-TENG sensor with different precisions (2°, 5°, and 10°) but same rotation angle and angular velocity (30° and 45° s<sup>-1</sup>). f) Calculated positions and g) angular velocities from the experimental data in the diagram (e), and their comparisons with the pre-set value. Current signal generated at the DSA-TENG sensor with different temperatures h) and relative humidity j) but same motion conditions. i) and k) Calculated angular velocity from the experimental data in the diagram (h) and (j), and their comparisons with the pre-set value.

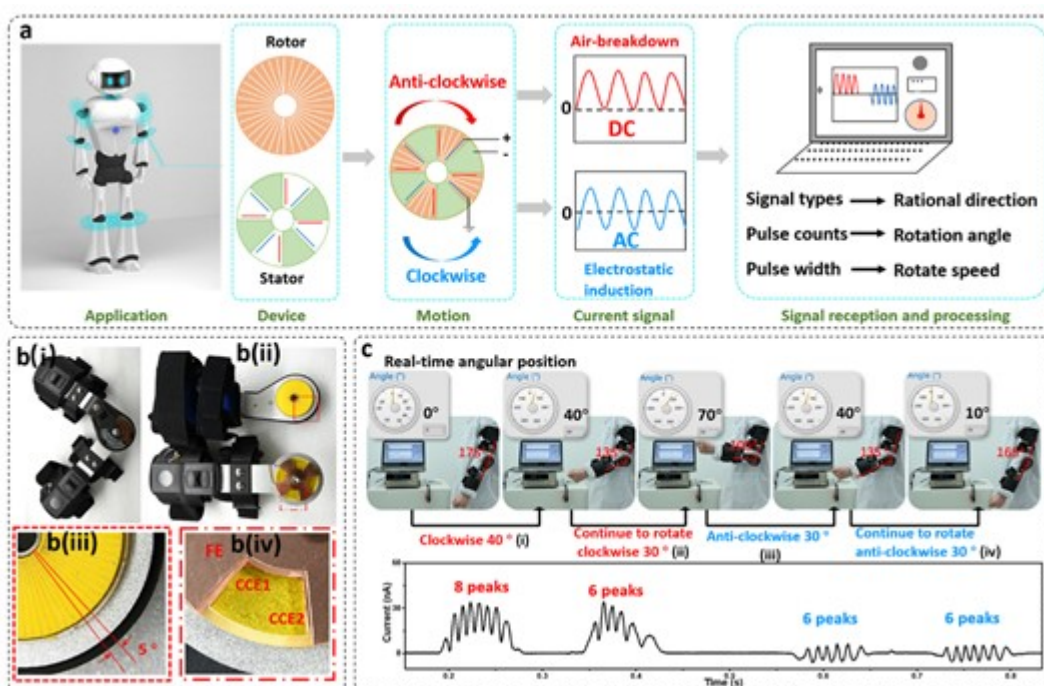


**Figure 4.** Application of DSA-TENG sensor in real-time monitoring in robotics. a) Schematic illustration of real-time monitoring the motion of robotic arm by DSA-TENG sensor. b) The digital photo of DSA-TENG sensor fixed on a person brace. c) The collected current data from DSA-TENG sensor when elbow bend with different angle.

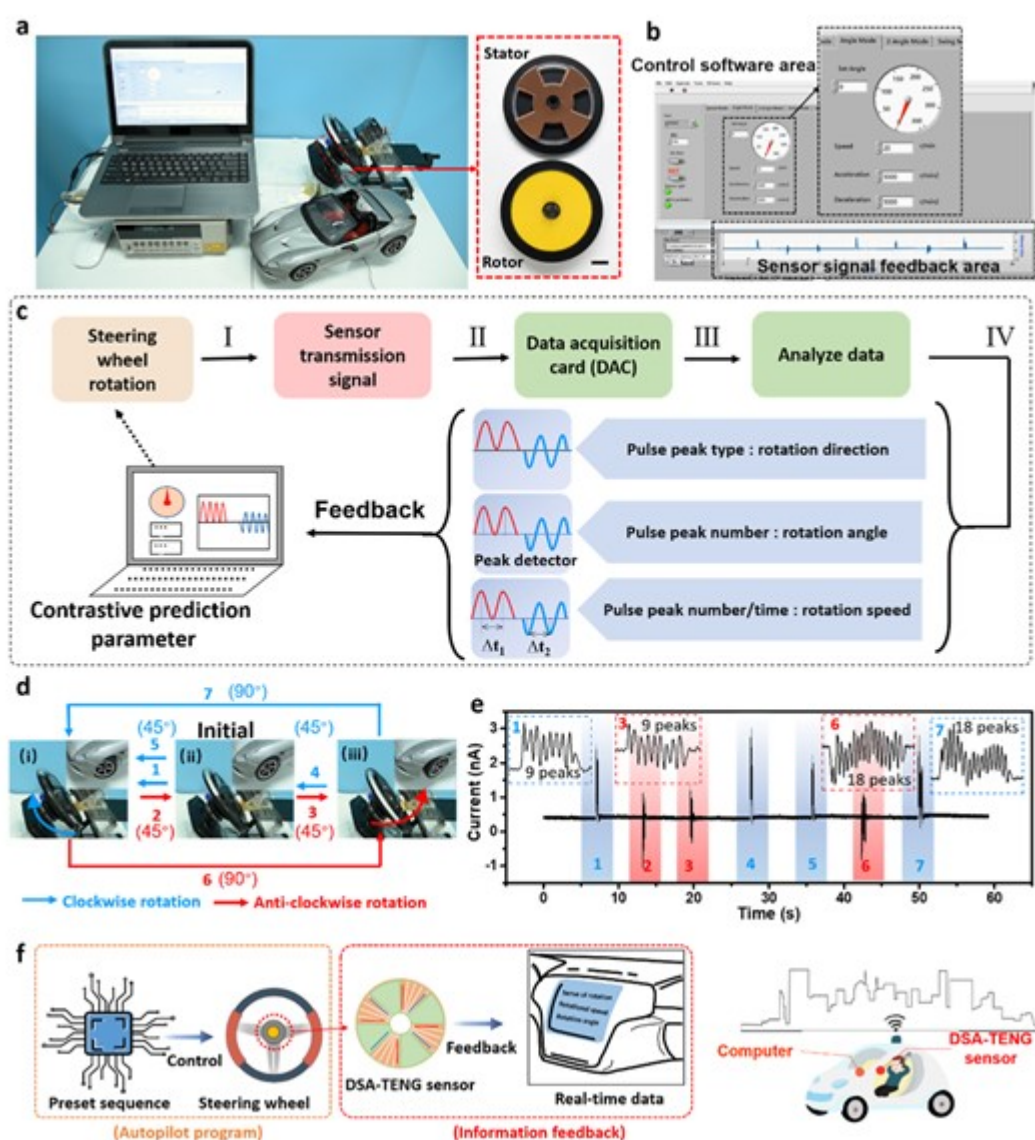


**Figure 5.** Application of DSA-TENG sensor in real-time monitoring in driverless car. a) The demonstration of rotation motion monitoring system, which is consist of a steering wheel equipped with DSA-TENG sensor, a remote-controlled car, a computer and an electrometer. b) The magnified image of the operational software in the diagram (a), scale bar 1 cm. c) Schematic illustration of real-time monitoring the motion of steering wheel by DSA-TENG sensor. d) The digital photo of the front wheels in various steer directions, and the

---

corresponding collected current data e) by DSA-TENG sensor during the change of rotation direction. f) The potential application of DSA-TENG sensor in driverless.

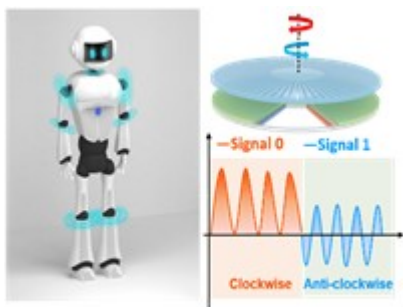
**The Table of Content Entry:** A self-powered dual-type signal vector sensor is designed by integrating an alternating current TENG and a direct current TENG, which achieves a high sensing precision and stability, provides an effective movement direction recognition method by self-powered switching of signal type in real-time motion monitoring of mechanical arm and automatic steering wheel.

**Keywords:** self-powered vector sensor, real-time monitoring vector movement, triboelectric nanogenerator, automatic robotics, automatic vehicle.

Shaoxin Li, Zhihao Zhao, Di Liu, Jie An, Yikui Gao, Linglin Zhou, Yanhong Li, Shengnan Cui, Jie Wang\*, Zhong Lin Wang\*

## **A Self-Powered Dual-Type Signal Vector Sensor for Smart Robotics and Automatic Vehicle**

**ToC Figure:**



- ✓ Self-power
- ✓ Directly judge the motion direction